Large-Scale Brain Networks Are Distinctly Affected in Right and Left Mesial Temporal Lobe Epilepsy

Brunno Machado de Campos, Ana Carolina Coan, Clarissa Lin Yasuda, Raphael Fernandes Casseb,* and Fernando Cendes*

Neuroimaging Laboratory, Department of Neurology, University of Campinas, Campinas, São Paulo, Brazil

Abstract: Mesial temporal lobe epilepsy (MTLE) with hippocampus sclerosis (HS) is associated with functional and structural alterations extending beyond the temporal regions and abnormal pattern of brain resting state networks (RSNs) connectivity. We hypothesized that the interaction of large-scale RSNs is differently affected in patients with right- and left-MTLE with HS compared to controls. We aimed to determine and characterize these alterations through the analysis of 12 RSNs, functionally parceled in 70 regions of interest (ROIs), from resting-state functional-MRIs of 99 subjects (52 controls, 26 right- and 21 left-MTLE patients with HS). Image preprocessing and statistical analysis were performed using UF^{2}C-toolbox, which provided ROI-wise results for intranetwork and internetwork connectivity. Intranetwork abnormalities were observed in the dorsal default mode network (DMN) in both groups of patients and in the posterior salience network in right-MTLE. Both groups showed abnormal correlation between the dorsal-DMN and the posterior salience, as well as between the dorsal-DMN and the executive-control network. Patients with left-MTLE also showed reduced correlation between the dorsal-DMN and visuospatial network and increased correlation between bilateral thalamus and the posterior salience network. The ipsilateral hippocampus stood out as a central area of abnormalities. Alterations on left-MTLE expressed a low cluster coefficient, whereas the altered connections on right-MTLE showed low cluster coefficient in the DMN but high in the posterior salience regions. Both right- and left-MTLE patients with HS have widespread abnormal interactions of large-scale brain networks; however, all parameters evaluated indicate that left-MTLE has a more intricate bihemispheric dysfunction compared to right-MTLE. *Hum Brain Mapp 37:3137–3152, 2016*.

Key words: functional connectivity; functional magnetic resonance imaging; default mode network; salience network; hippocampus; visuospatial network

Contract grant sponsor: FAPESP (São Paulo Research Foundation); Contract grant number: 2013/00099-7, 2013/07559-3, and 2014/15918-6

Correction added on 06 June 2016, after first online publication.

*Correspondence to: Fernando Cendes, Departamento de Neurologia, Faculdade de Ciências Médicas – UNICAMP, Cidade Universitária Zeferino Vaz, Campinas SP, Brazil, CEP 13083-970. E-mail: fcendes@unicamp.br

Conflicts of Interest: None of the authors has any conflict of interest to disclose. We confirm that we have read the Journal's position on issues involved in ethical publication and affirm that this report is consistent with those guidelines.

Received for publication 14 January 2016; Revised 4 April 2016; Accepted 15 April 2016.

DOI: 10.1002/hbm.23231

Published online 2 May 2016 in Wiley Online Library (wileyonlinelibrary.com).

INTRODUCTION

Mesial temporal lobe epilepsy (MTLEs) is associated with functional and structural changes that extend beyond the temporal regions [Holmes et al., 2013; Liu et al., 2012]. Hippocampus sclerosis (HS) is the hallmark of most MTLE [Cendes et al., 1993] and studies indicate that MTLE with HS involves a complex pattern of brain functional and structural alterations [Campos et al., 2015 ; Holmes et al., 2013; Pittau et al., 2012]. Functional magnetic resonance imaging (fMRI) during task-free conditions has been widely used to portray functional network characteristics in both normal and pathological conditions [Seeley et al., 2009], including MTLE. Different studies have investigated the impact of MTLE on these resting state networks (RSNs) [Bettus et al., 2009; Cataldi et al., 2013; Haneef et al., 2014; Laufs et al., 2007; Liao et al., 2010], including analysis of specific networks such as the default mode network (DMN) and the salience network. [Zhang et al., 2010].

Other studies have used different approaches (i.e., ICA, seed-based connectivity) to explore some specific RSNs such as the DMN [Liao et al., 2011], perceptual [Zhang et al., 2009a], and attention networks [Zhang et al., 2009b]. These studies revealed altered networks, compared to controls. The overall activation of DMN in MTLE is apparently reduced, as well as the functional connectivity between its nodes [Liao et al., 2011]. Some of these studies also demonstrated that MTLE affects the attention networks and perceptual networks, resulting in significant abnormal impairment between their regions [Cataldi, et al., 2013]. These findings could explain the worst performances of these patients on cognitive tasks as memory and language, as well as on auditory and visual naming activities [Alessio et al., 2006; Vannest et al., 2008].

Given the characteristics of a network-level pathology in MTLE [Spencer, 2002], other studies have examined graph-theory properties [Bullmore and Sporns, 2009] of both structural [Bernhardt et al., 2011; Bonilha et al., 2013] and functional data [Chiang et al., 2014; Liao et al., 2010; Vlooswijk et al., 2011]. These studies evaluated the relationships between the syndrome alterations and properties such as degree of connectivity, clustering coefficient and hub distribution, demonstrating alterations in MTLE characterized by reduced specificity and global efficiency [Bernhardt et al., 2011; Liao et al., 2010]. Most of the previous graph theory studies in MTLE have applied anatomical parcellation to functional maps and compared differences between right and left MTLE groups in comparison to controls [Bettus et al., 2009; Wang et al., 2009]. The use of functional parcellation aims to improve the access to alterations on the cerebral functional organization. Since we can define the brain functional networks as inherent patterns of areas dynamically correlated during a specific task or at rest [Eguíluz et al., 2005], the direct study of these patterns and the interaction of its subareas could improve the identification of changes related to abnormal behavior, or secondary to neurological diseases.

Despite the information about specific RSNs in MTLE, there is no current data about how these networks interact in this condition and whether this interaction differs between patients with right or left HS. As mentioned before, it is well-known that patients with left MTLE have worse performance in memory tasks and distinct structural damage of cerebral gray and white matter than patients with right MTLE [Besson et al., 2014; Keller et al., 2002; Riederer et al., 2008]. These data put together implies that right and left MTLE could have different pathological mechanisms. Although previous studies have focused on the differences in functional connectivity between these groups of patients, these analyses were restricted to specific brain nodes, more often including the hippocampal region [Morgan et al., 2012; Pereira et al., 2010; Zhang et al., 2010]. However, today it is accepted that in order to understand the brain function and its disruptions, we must move forward from looking at specific brain regions and try to understand how the different areas interact and the possible abnormalities of this interaction. Therefore, the study of intercorrelations among RSNs in right and left MTLE might improve the understanding of the underlying mechanisms associated with these conditions.

We hypothesized that internetwork and intranetwork connectivity of RSNs is differently altered in patients with right and left MTLE compared to controls. In order to investigate that, we studied connectivity between RSNs using regions of interest (ROIs) derived from a functional parcellation in homogeneous groups of MTLE patients with unilateral HS.

METHODS

Subjects

All patients and controls included in this study signed an informed consent, approved by the Ethics Committee of the University of Campinas.

We included 47 consecutive adult patients with clinical and electroencephalographic diagnosis of drug-resistant MTLE and MRI signs of unilateral HS followed at the Epilepsy Clinic of the University of Campinas. The clinical diagnosis of MTLE was based on ILAE criteria [Berg et al., 2010]. All patients had seizure semiology compatible with seizure onset in the mesial temporal structures and had failed at least two antiepileptic drugs at the moment of the enrollment in this study. All underwent extensive interictal and/or ictal scalp EEG recordings, with epileptiform abnormalities restricted to the anterior and medial temporal electrodes. MRI scans acquired with a protocol for epilepsy were reviewed by two different epileptologists (FC and ACC) looking for signs of HS (clear loss of internal structure and volume reduction on T1 weighted image (WI) and signal hyperintensity on T2 WI/FLAIR). Second, MRI signs of HS were confirmed through quantification of volume and T2 signal according to our center protocol

TABLE I. Demographic and clinical information

Group	Controls	R-MTLE	L-MTLE
Age (years)	43 (±13)	46 (±7)	47 (±6)
Female	52%	58%	48%
Seizure onset (years)		12 (±9)	8 (±7)
Epilepsy duration (years)		33 (±11)	39 (±9)
Familiar history of epilepsy		50%	45%
Protocol type (P1/P2)	26/26	20/6	15/6

For "Age," "Seizure Onset," and "Epilepsy Duration," the values represent the mean and the standard deviation. In the fields "Female" and "Family History," the values represent the percentage of occurrence of these factors in each group.

[Coan et al., 2014b]. In this study, patients classified with bilateral HS were not selected. According to the side of the HS and the ictal/interictal EEG abnormalities, patients were classified as right (R-MTLE) or left (L-MTLE) MTLE. Only patients with concordant laterality on MRI and EEG were selected.

MRI Acquisitions

All patients and controls underwent 3-tesla MRI (Philips Achieva) according to the following protocol:

1. Structural images: T1 WI with isotropic voxels of 1 mm, acquired in the sagittal plane, 180 slices, 1 mm thick, no gap, flip angle = 8°, TR = 7.0 ms, TE = 3.2 ms, FOV = 240 × 240 mm^2.
2. Functional images: patients and controls were submitted to either one of two distinct functional protocols: P1) echo planar image (EPI) with isotropic voxel of 3 mm, acquired on the axial plane with 32 slices, gap of 0.3 mm, matrix = 80 × 80, flip angle = 75°, TR = 2 s, TE = 30 ms, in a 6 min scan resulting in 180 dynamics; P2) EPI with isotropic acquisition voxel of 3 mm, acquired on the axial plane with 39 slices, no gap, matrix = 80 × 80, flip angle = 90°, TR = 2 s, TE = 30 ms in a 6 min scan resulting in 180 dynamics. The main difference between protocols was the coverage of inferior cerebellar regions. Therefore, we did not include the inferior cerebellum in the analyses as described below.

In total, we selected 99 subjects according to clinical, demographic and MRI parameters (Table I): 52 controls, 26 patients with R-MTLE, and 21 patients with L-MTLE.

There was no difference between the groups considering age and gender. Significant differences were observed only between controls and R-MTLE group on the proportion of the protocol types (pairwise Fisher's Exact Test, two-tailed *P*-value = 0.028); therefore, this was considered as a covariate on the analysis.

Additionally, we found no differences between patients groups regarding age at seizures onset, duration of epilepsy and family history of epilepsy.

Functional Connectivity

The UF²C—user friendly functional connectivity toolbox

The UF²C toolbox (http://www.lni.hc.unicamp.br/app/uf2c/) was developed by the author (Campos, BM) aiming to standardize and facilitate connectivity studies through a straightforward graphical user interface and validated preset parameters. The toolbox runs within MATLAB platform (2014b, The MathWorks) with SPM12 (Statistical Parametric Mapping 12, http://www.fil.ion.ucl.ac.uk/spm/) and it is freely available for download.

We preprocessed and performed the statistical analysis (first and second level) according to the UF²C standard pipeline. The preprocessing was based on: fMRIs dynamics realignment (using mean image as reference), images coregistration (fMRI mean image with T1 WI), spatial normalization (MNI-152), smoothing (kernel of 6 × 6 × 6 mm^3 at FWHM) and T1 WI tissue segmentation (gray matter [GM], white matter [WM], and cerebral spinal fluid [CSF]) and normalization (MNI-152). The segmented GM maps were interpolated to match the functional images and used to mask the analysis, removing non-GM regions. Additionally, we regressed out six head motion parameters (three rotational and three translational) as well as WM and CSF average signals. Finally, we detrended (removed linear trends) and band-pass filtered (0.008–0.1 Hz) the time-series. The Figure 1 is a flowchart representing all the processing steps.

ROI and cross-correlation matrices

For the first level analysis, we generated individual matrices based on ROIs derived from a functional parcellation. Instead of applying anatomical parcellation as seen in previous studies, we used 70 ROIs from 12 functional networks previously created and described by Shirer et al [2012]: *Anterior Salience* (network code = n1, number of ROIs = 5), *Posterior Salience* (network code = n2, number of ROIs = 10), *Basal Ganglia* (network code = n3, number of ROIs = 4), *Dorsal DMN* (network code = n4, number of ROIs = 9) *Ventral DMN* (network code = n5, number of ROIs = 9) left executive-control network (ECN) (network code = n6, number of ROIs = 5), right *ECN* (network code = n7, number of ROIs = 5), *Auditory* (network code = n8, number of ROIs = 2), *Visual* (network code = n9, number of ROIs = 3), *Language* (network code = n10, number of ROIs = 6), *Sensorimotor* (network code = n11, number of ROIs = 4), and *Visuospatial/Dorsal Attention* (network code = n12, number of ROIs = 8). We selected these ROIs to evaluate functional connectivity in widespread brain areas considering distributed relevant functional networks. The Visual network in this study is the

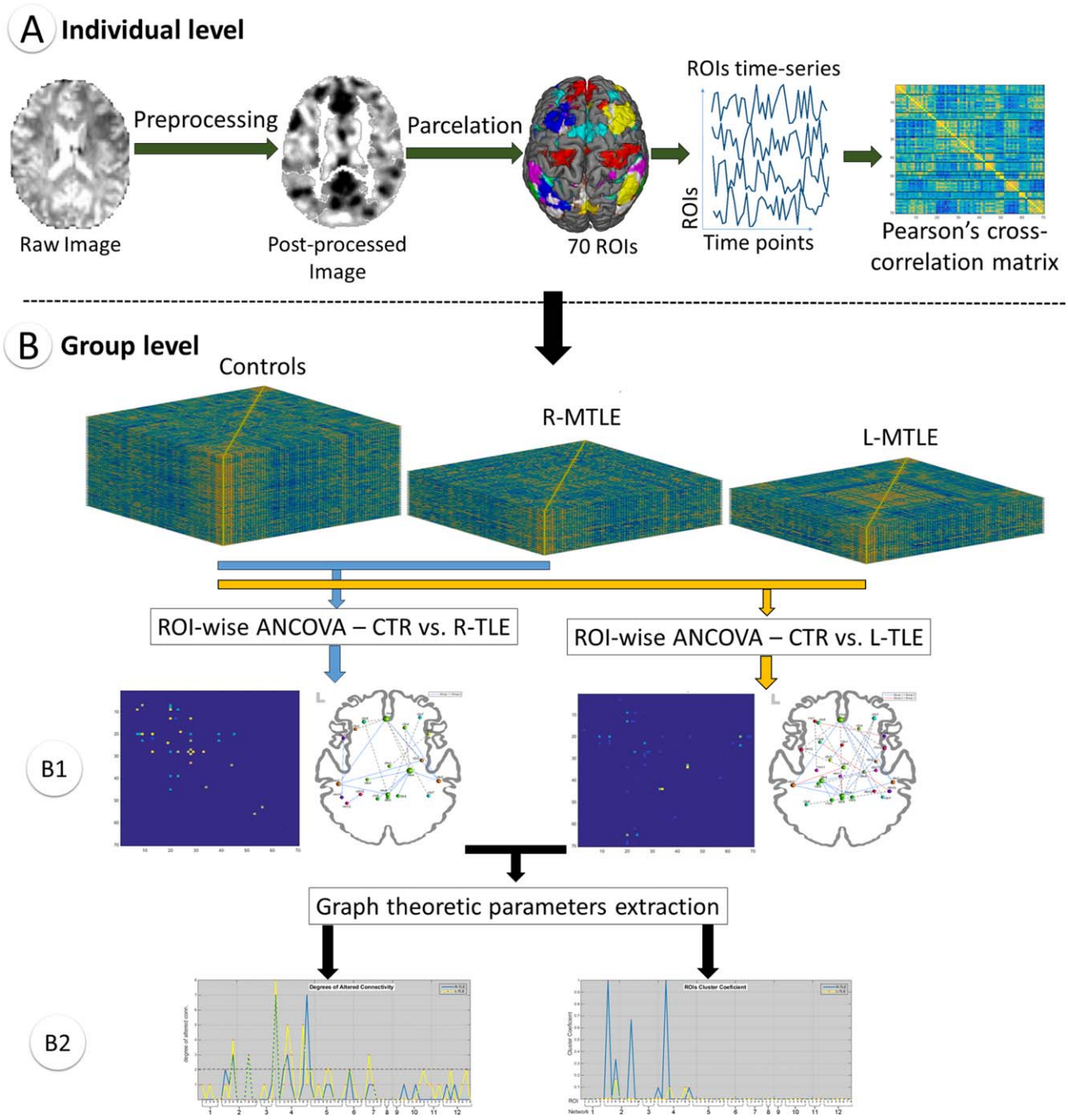

Figure 1.

Pre- and post-processing flowchart for first and second statistical levels. The part "**A**" describes all individual steps included in the first level statistical analysis. The part "**B**" describes the group level statistical and graph-theory analysis. ROIs: regions of interest; R-MTLE: right mesial temporal lobe epilepsy; L-MTLE: left mesial temporal lobe epilepsy; CTR: control group.

union of the ROIs from the High and Prime visual networks described by Shirer et al [2012].

As we observed FOV variations between functional protocols in the inferior portion of the cerebellum, no ROIs from this area were included to avoid data from the bottom of the images. Therefore, in our analysis, we excluded the following ROIs due to their positioning on the inferior portion of the cerebellum: two ROIs from the Anterior

Salience network (ROIs 6 and 7); two from the Posterior Salience (ROIs 8 and 11); one from Basal Ganglia (ROI 5); one from Language (ROI 7); one from LECN (ROI 5); one from RECN (ROI 5); two from Sensorimotor (ROIs 4 and 6); one from ventral DMN (10); and three from Visuospatial (ROIs 9, 10, and 11). Additionally, one ROI was excluded due to its small size: Visual (prime visual 2) with four voxels.

Time-series were consistently extracted from each ROI of each subject. For a specific ROI, we used the average time series of all ROI voxels that matched two consecutive criteria:

a. Being included on the subject GM mask;
b. The UF^{2}C correlates each single ROI voxel time series with the average ROI time series (GM-masked). The voxel was included (to the average) if its correlation value is within the average ± standard deviation of all correlations between the ROI-masked voxels.

The cross-correlation matrices were created by performing Pearson's correlation tests (2,415 tests, pairwise combination of all the 70 ROIs, removing auto [diagonal] and symmetric correlations). These individual correlation matrices were subsequently converted to *z*-score (Fisher's Z-transformation) and taken to a second level analysis to investigate differences between controls and patients groups.

Group comparisons

The second level analyses were performed also using an appropriate modality on UF^{2}C toolbox. As a first step, to evaluate confounding effects induced by the two different fMRI acquisition protocols, we performed an additional test, comparing only control subjects, who were divided into two groups with pure protocol types (26 controls with protocol type "P1" and 26 with protocol type "P2"). No significant differences were detected between these groups of control subjects (alpha = 0.05, false discovery rata [FDR] corrected).

In order to evaluate and characterize how right or left MTLE functionally affects the RSN behaviors and interactions, we evaluated inter-ROIs connectivity considering the internetwork (among ROIs of different networks) and intranetwork (among ROIs of a same network) interactions. For that, we performed MANCOVA tests, with a protocol type variable as covariate and alpha = 0.0375 (due to the two multiple pairwise group comparisons – FDR correction). All tests between ROIs (2,415 tests) were also corrected for multiple comparisons using the FDR procedure [Benjamini, and Hochberg, 1995] and only corrected sub threshold results ($P < 0.0375$) were considered significant.

It is important to highlight and clarify some terms applied in this study. "Relative decreased connectivity" (Fig. 2A,B) and "relative increased connectivity" (Fig. 2C,D) indicate lower or higher absolute Person's correlation scores of patients compared to the control group's respective scores. In this sense, the idea of "decreased" or "increased" means that the Person's correlation values are, respectively, farther or closer to zero when compared to controls, regardless of whether the correlation is positive (Fig. 2A,C) or negative (Fig. 2B,D). Interestingly, we also detected some situations in which the correlation scores from patients presented opposite signals compared to controls. Despite the usage of absolute *r*-score values to define the direction of the differences among groups, the statistical tests were performed with the original values (transformed to *z*-score, but keeping the original signals), making sure that comparisons among correlations in opposite directions (Fig. 2E,F) have been considered accordingly in the statistical analysis. For these scenarios, the graphical results (Fig. 3) do not show these alterations as decreased or increased, but just indicate them with dashed lines.

Aiming to characterize how the connectivity alterations are laterally distributed, we calculated a laterality index (LI). We subtracted the number of contralateral altered connections (CAC), from the number of ipsilateral altered connections (IAC) and divided it by the total number of altered connections [Coito et al., 2015]:

$$LI = \frac{IAC\text{-}CAC}{IAC+CAC}$$

The interpretation of the LI value could be summarized as follows: if the alterations are completely restricted to the ipsilateral side, its LI value is 1. Values between 0 and 1 reveals that the majority of the alterations is ipsilateral and the value oscillates within this range according to the weight (number) of the contralateral alterations. Analogously, the LI is negative if the majority of the alterations is on the contralateral side, varying between −1 and 0 according to the weight (number) of the ipsilateral alterations. If all alterations are restricted to the contralateral side, the LI value would be −1. It is important to clarify that in the case of alterations including a interhemispheric ROI and a non-interhemispheric ROI, we consider the alteration side to be the same as the non-interhemispheric ROI. Another important observation is that since the LI uses the total number of alterations as equation denominator, the resultant LI value quickly decreases (non-linearly) due to the less altered side weight.

Graph theory parameters

We performed an additional analysis to extract three graph theory parameters of altered connectivity. We calculated them using the results of the statistical differences between groups, generating graph information related to the connectivity alterations for R-MTLE and L-MTLE. (1) The ROIs degree of altered connectivity (RDAC), which

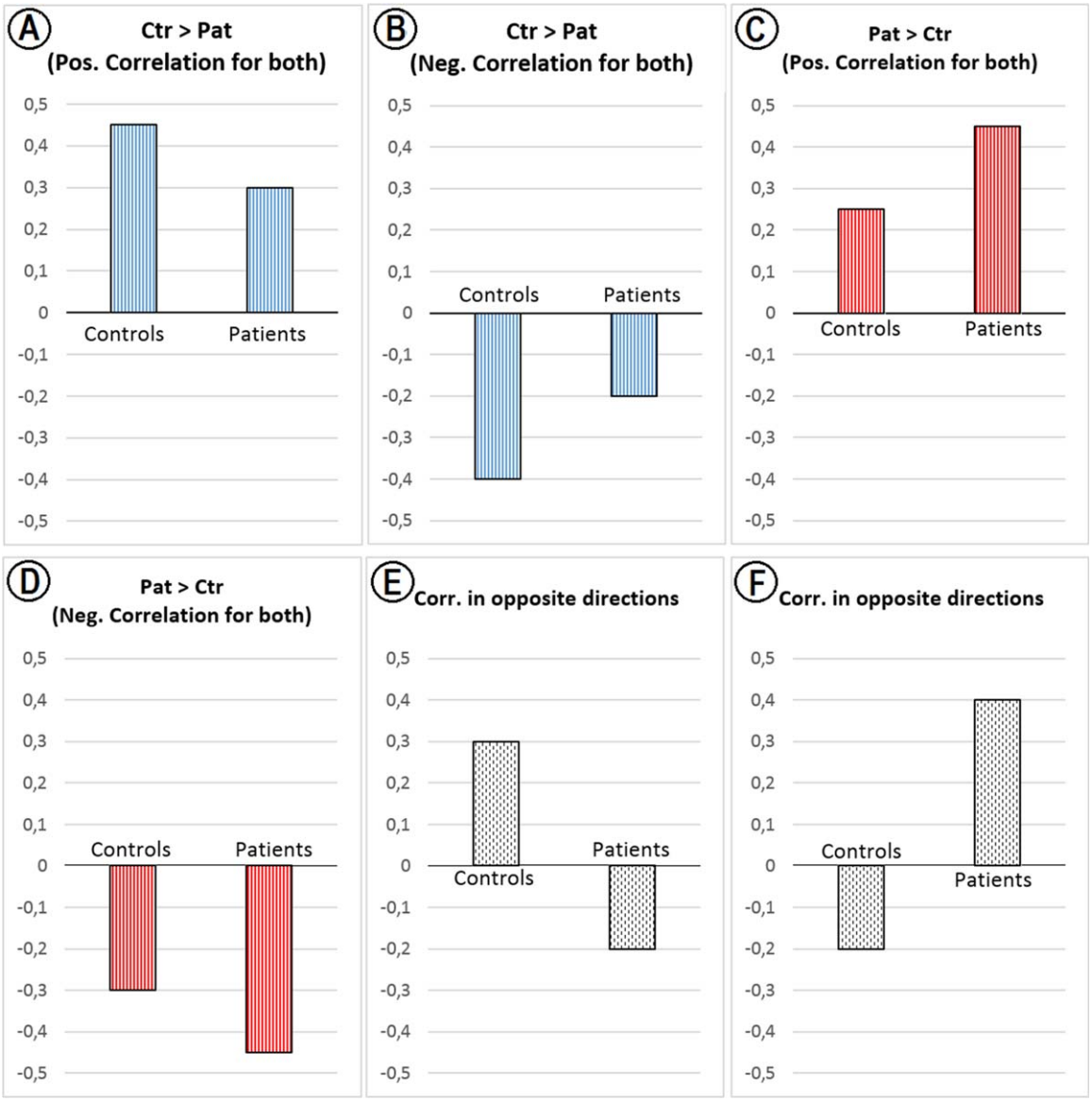

Figure 2.

Illustrative examples of possible connectivity results comparing controls and patients average scores. In "**A**," controls and patients have positive correlations between two regions and the control group presents a higher value. In "**B**," controls and patients presents negative correlations among two regions and controls showed a higher (absolute) value. The results exemplified in "A" and "B" are represented with blue lines on Figure 3. In "**C**" and "**D**," examples similar to "A" and "B," but in both, patients presented higher absolute correlations values. The results exemplified in "C" and "D" are represented with red lines on Figure 3. Finally, in "**E**" and "**F**" we are showing examples of connections with distinct directions (positive for one group and negative to another). The results exemplified in "E" and "F" are represented with dashed lines on Figure 3. Ctr: control group; Pat: patients; Pos.: positive; Neg.: negative; Corr: correlation.

means the total number of significant altered connections of each ROI, calculated for each patient group separately. The RDAC provides an overall idea about the significance of a specific altered node, illustrating if it is merely an affected part of a net of alterations (low RDAC) or a center of these alterations (high RDAC). In line with that, the RDAC can be understood as a measure of centrality. (2) The average degree of altered connectivity (ADAC) which considers the RDACs of both patient groups together, calculating an overall average among them:

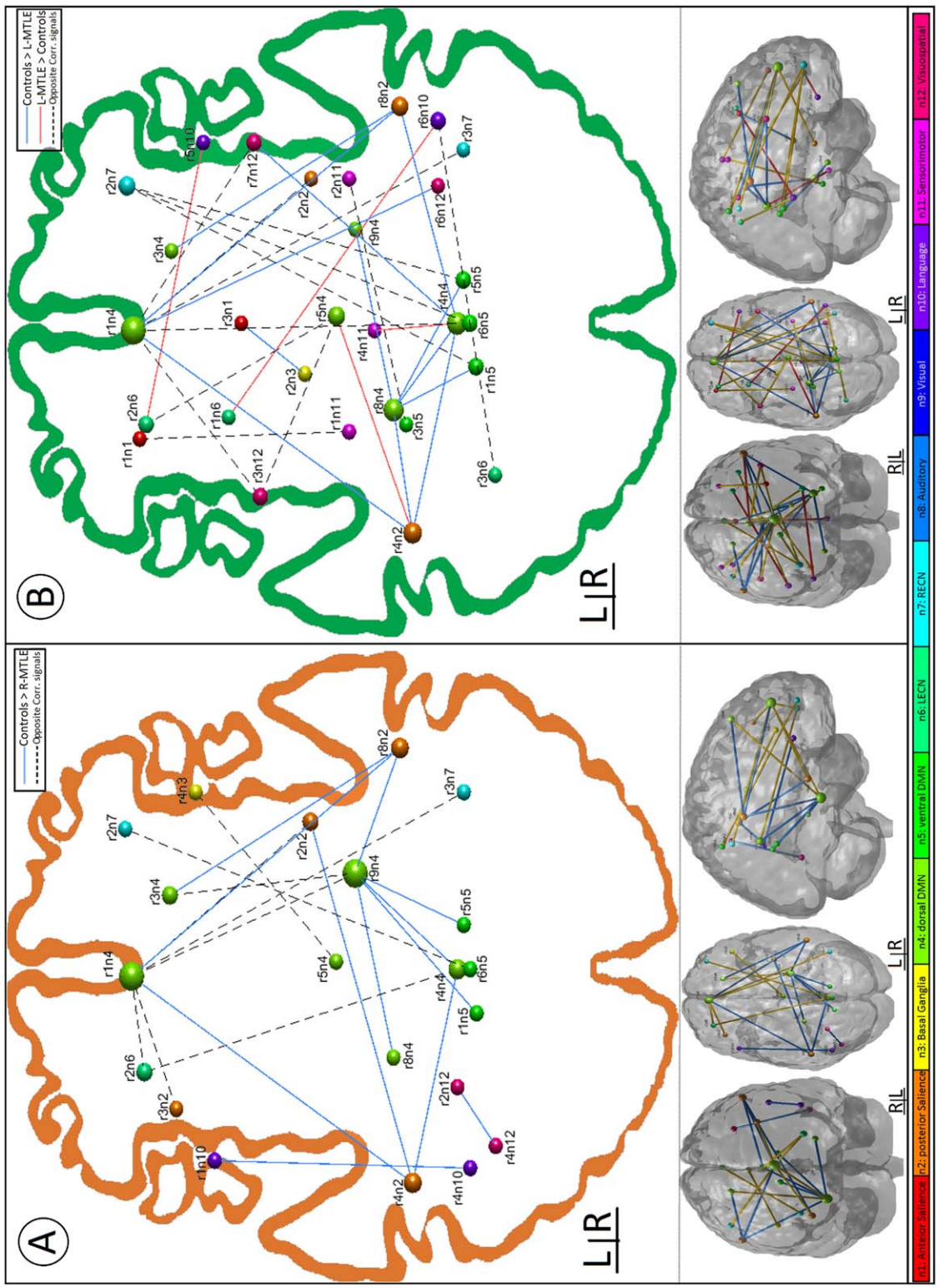

Figure 3.

Altered connections on right and left MTLE when compared to control group (ANCOVA test, $P < 0.0375$ false discovery rate [FDR] corrected). (**A**) Altered connections on R-MTLE. The blue lines indicate pairs of ROIs with relative decreased connectivity. The dashed lines (or yellow on the 3D brain) indicate connections with opposite correlation signal in R-MTLE when compared to controls. (**B**) Altered connections on L-MTLE. The blue lines indicate pairs of ROIs with decreased connectivity. The red lines indicate pairs of ROIs with relative increased connectivity. The dashed lines (or yellow on the 3D brain) indicate connections with opposite correlation signal on L-MTLE when compared to controls. The spheres sizes are in function of the degree of altered connectivity and their colors represent the different networks. R-MTLE: right mesial temporal lobe epilepsy; L-MTLE: left mesial temporal lobe epilepsy; Corr: correlation; L: left side; R: right side; DMN: default mode network; LECN: left executive control network; RECN: right executive control network.

TABLE II. Relative decreased connectivity Hubs on R-MTLE

Hub (ROI/Region)	ROI name	Network	Anatomical regions	ROI (%)	Voxel (*n*)
r4n2	r1n4	Dorsal DMN	Medial Frontal Gy.	42	2233
L. Supramarginal Gy.			Anterior Cingulate	21	1148
L. Inf. Parietal Gy.	r4n4	Dorsal DMN	Post. Cingulate	33	525
(Post. Salience)			Precuneus	31	497
	r2n2	Post. Salience	R. Insula	35	134
			R. Sup. Temporal Gy.	14	19
r8n2	r1n4	Dorsal DMN	Medial Frontal Gy.	42	2233
R. Poscentral Gy.			Anterior Cingulate	21	1148
R. Supramarginal Gy.	r3n4	Dorsal DMN	R. Sup. Frontal Gy.	90	124
(Post. Salience)	r9n4	Dorsal DMN	R. Hippocampus	97	139
r1n4	r4n2	Post. Salience	L. Supramarginal Gy.	50	660
Sup. Frontal Gy.			L. Inf. Parietal Gy.	32	389
Medial Frontal Gy.	r8n2	Post. Salience	R. Poscentral Gy.	32	327
(Dorsal DMN)			R. Supramarginal Gy.	11	112
r9n4	r8n2	Post. Salience	R. Poscentral Gy.	32	327
R. Hippocampus			R. Supramarginal Gy.	11	112
(Dorsal DMN)	r4n4	Dorsal DMN	Post. Cingulate	33	525
			Precuneus	31	497
	r8n4	Dorsal DMN	L. Hippocampus	87	342
	r1n5	Ventral DMN	Post. Cingulate	54	251
			L. Calcarine	46	214
	r5n5	Ventral DMN	Post. Cingulate	58	345
			R. Precuneus	47	278

The "voxel (*n*)" indicates the number of voxels of the respective anatomical region and the "ROI (%)" the percentage of this region within the original ROI mask. R: right; L: left; r: ROI number; n: Network number; Gy: gyrus; DMN: default mode network; Sup: superior; Post: posterior.

$$\mathrm{ADAC} = \frac{\sum_{i=1}^{n_1} \mathrm{RDAC}_i + \sum_{j=1}^{n_2} \mathrm{RDAC}_j}{n_1 + n_2},$$

where i and j are the indexes of the ROIs with altered connections for R-MTLE and L-MTLE respectively; and the n_1 and n_2, the total number of altered ROIs for R-MTLE and L-MTLE respectively. For further reference, we considered a ROI as a hub of alterations, if its RDAC was greater than the ADAC value. (3) The clustering coefficient of altered connectivity (CCAC):

$$CCAC_i = \frac{t_i}{RDAC_i \times \frac{(RDAC_i - 1)}{2}},$$

where i is the ROI index and t, the total number of triangles (connections between ROI i neighbors'). The CCACs, similarly to the RDACs are calculated for each altered

TABLE III. Opposite connectivity Hubs on R-MTLE

Hub (ROI/Region)	ROI name	Network	Anatomical regions	ROI (%)	Voxel (*n*)
r1n4	r2n2	Post. Salience	R. Insula	35	134
Sup. Frontal Gy.			R. Sup. Temporal Gy.	14	19
Medial Frontal Gy.	r3n2	Post. Salience	L. Middle Frontal Gy.	91	93
(Dorsal DMN)	r9n4	Dorsal DMN	RT. Hippocampus	97	139
	r2n6	L. ECN	L. Middle Frontal Gy.	60	264
			L. Inf. Frontal Gy.	22	98
	r3n7	R. ECN	R. Angular Gy.	38	715
			R. Supramarginal Gy.	12	228
r9n4	r1n4	Dorsal DMN	Medial Frontal Gy.	42	2233
R. Hippocampus			Anterior Cingulate	21	1148
(Dorsal DMN)	r3n4	Dorsal DMN	R. Sup. Frontal Gy.	90	124

The "voxel (*n*)" indicates the number of voxels of the respective anatomical region and the "ROI (%)" the percentage of this region within the original ROI mask. R: right; L: left; r: ROI number; n: network number; Gy: gyrus; DMN: default mode network; Post: posterior; Sup: superior; Inf: inferior; ECN: executive control network.

TABLE IV. Relative decreased connectivity Hubs on L-MTLE

Hub (ROI/Region)	ROI name	Network	Anatomical regions	ROI (%)	Voxel (*n*)
r4n2	r1n4	Dorsal DMN	Medial Frontal Gy.	42	2233
L. Supramarginal Gy.			Anterior Cingulate	21	1148
L. Inf. Parietal Gy.	r4n4	Dorsal DMN	Post. Cingulate	33	525
(Post. Salience)			Precuneus	31	497
	r8n4	Dorsal DMN	L. Hippocampus	87	342
r8n2	r1n4	Dorsal DMN	Medial Frontal Gy.	42	2233
R. Poscentral Gy.			Anterior Cingulate	21	1148
R. Supramarginal Gy.	r3n4	Dorsal DMN	R. Sup. Frontal Gy.	90	124
(Post. Salience)	r4n4	Dorsal DMN	Posterior Cingulate	33	525
			Precuneus	31	497
r1n4	r4n2	Post.Salience	L. Supramarginal Gy.	50	660
Sup. Frontal Gy.			L. Inf. Parietal Gy.	32	389
Medial Frontal Gy.	r8n2	Post.Salience	R. Poscentral Gy.	32	327
(Dorsal DMN)			R. Supramarginal Gy.	11	112
	r6n12	Visuospatial	R. Inf. Parietal lobe	28	329
			R. Sup. Parietal lobe	21	254
r4n4	r4n2	Post.Salience	L. Supramarginal Gy.	50	660
Post. Cingulate			L. Inf. Parietal Gy.	32	389
Precuneus	r8n2	Post.Salience	R. Poscentral Gy.	32	327
(Dorsal DMN)			R. Supramarginal Gy.	11	112
	r8n4	Dorsal DMN	L. Hippocampus	87	342
	r7n12	Visuospatial	R. Inf. Frontal Gy.	61	201
r8n4	r4n2	Post.Salience	L. Supramarginal Gy.	50	660
L. Hippocampus			L. Inf. Parietal Gy.	32	389
(Dorsal DMN)	r4n4	Dorsal DMN	Post. Cingulate	33	525
			Precuneus	31	497
	r9n4	Dorsal DMN	R. Hippocampus	97	139
	r1n5	Ventral DMN	Post. Cingulate	54	251
			L. Calcarine	46	214
	r5n5	Ventral DMN	Post. Cingulate	58	345
			R. Precuneus	47	278

The "voxel (*n*)" indicates the number of voxels of the respective anatomical region and the "ROI (%)" the percentage of this region within the original ROI mask. R: right; L: left; r: ROI number; n: network number; Gy: gyrus; DMN: default mode network; Sup: superior; Inf: inferior; Post: posterior.

ROI, from each patient group separately. The CCAC indicates how an altered ROI and its neighbors (via altered connections) are segregated (low CCAC) or interlaced (high CCAC) among themselves. It may indicate the existence of a net of alterations. The standard definition of these and other several graph parameters were fully described by Rubinov and Sporns [2010].

RESULTS

Table I shows the detailed clinical characteristics of MTLE patients. No significant differences (alpha = 0.03 FDR corrected) were observed between R-MTLE and L-MTLE regarding distribution of gender ($P = 0.609$), age ($P = 0.675$), age of seizure onset ($P = 0.0798$), epilepsy duration ($P = 0.072$), or family history of epilepsy ($P = 0.743$).

Compared to controls, both patients groups (R-MTLE and L-MTLE) presented functional connectivity alterations on the pairwise ROIs analysis (alpha = 0.0375 FDR corrected). From the 12 studied networks, just the auditory and visual networks did not present alterations, although for the R-MTLE group, the anterior salience and sensorimotor networks were also preserved. Tables (II–VI) show the results organized in hubs of alterations. The ROIs anatomical labeling was performed using xjView toolbox (http://www.alivelearn.net/xjview).

R-MTLE Connectivity

In total, 21 ROIs linked by 21 connections showed alterations on R-MTLE group when compared to controls. We found significant connectivity decreases in R-MTLE mainly on the right hippocampus (r9n4) connections with dorsal and ventral DMN (n4 and n5) and posterior salience

TABLE V. Relative increased connectivity Hubs on L-MTLE

Hub (ROI/Region)	ROI name	Network	Anatomical regions	ROI (%)	Voxel (*n*)
r4n2 L. Supramarginal Gy. L. Inf. Parietal Gy. (Post. Salience)	r5n4	Dorsal DMN	Bilateral Thalamus	47	105
r4n4 Post. Cingulate Precuneus (Dorsal DMN)	r4n11	Sensorimotor	Cerebelum	75	2015
r5n4 Bilateral Thalamus (Dorsal DMN)	r4n2	Post.Salience	L. Supramarginal Gy. L. Inf. Parietal Gy.	50 32	660 389

The "voxel (*n*)" indicates the number of voxels of the respective anatomical region and the "ROI (%)" the percentage of this region within the original ROI mask. R: right; L: left; r: ROI number; n: network number; Gy: gyrus; DMN: default mode network; Sup: superior; Inf: inferior; Post: posteriorL: left; Gy: gyrus; DMN: default mode network; Post: posterior; Inf: inferior.

network (n2) (Table II and Fig. 3A in blue lines). Three other hubs presented relative decreased connectivity, including frontal portion of DMN (r1n4) and right and left posterior salience (r8n2 and r4n2).

In summary, by a network perspective, we observed decreased intranetwork connectivity between the posterior salience (n2) ROIs and also between dorsal DMN (n4) ROIs. Decreased internetwork connectivity were observed between posterior salience (n2) and dorsal DMN (n4) and also between dorsal DMN (n4) and ventral DMN (n5).

The R-MTLE group also showed opposite connectivity relative to controls including: frontal portion of the dorsal DMN (r1n4), the right hippocampus (r9n4), left and right ECN ROIs (r2n6 and r3n7), and anterior salience (r3n2). By a network perspective, we observed opposite intranetwork connectivity only between dorsal DMN (n4) ROIs and opposite internetwork connectivity affecting just the dorsal DMN (n4) and some of its connections with the posterior salience (n2), left ECN (n6), and right ECN (n7) (Table III and Fig. 3A in dashed lines).

Graph theory properties

On the R-MTLE, the ipsilateral hippocampus and the frontal portion of the DMN (r1n4) presented the highest

TABLE VI. Opposite connectivity Hubs on L-MTLE

Hub (ROI/Region)	ROI name	Network	Anatomical regions	ROI (%)	Voxel (*n*)
r1n4	r2n2	Post.Salience	R. Insula	35	134
Sup. Frontal Gy.			R. Sup. Temporal Gy.	14	19
Medial Frontal Gy.	r6n5	Ventral DMN	Precuneus	88	1703
(Dorsal DMN)	r3n7	R. ECN	R. Angular Gy.	38	715
			R. Supramarginal Gy.	12	228
	r3n12	Visuospatial	L. Inf. Frontal Gy.	67	748
	r7n12	Visuospatial	R. Inf. Frontal Gy.	61	201
r5n4	r2n6	L. ECN	L. Mid. Frontal Gy.	60	264
Bilateral Thalamus			L. Inf. Frontal Gy.	22	98
(Dorsal DMN)	r3n12	Visuospatial	L. Inf. Frontal Gy.	67	748
r2n7	r1n5	Ventral DMN	Post. Cingulate	54	251
R. Mid. Frontal Gy.			L. Calcarine	46	214
R. Sup. Frontal Gy.	r5n5	Ventral DMN	Post. Cingulate	58	345
(R. ECN)			R. Precuneus	47	278
	r6n5	Ventral DMN	Precuneus	88	1703

The "voxel (*n*)" indicates the number of voxels of the respective anatomical region and the "ROI (%)" the percentage of this region within the original ROI mask. R: right; L: left; Gy: gyrus; DMN: default mode network; Post: posterior; Inf: inferior; ECN: executive control network Sup: superior; Mid: Middle.

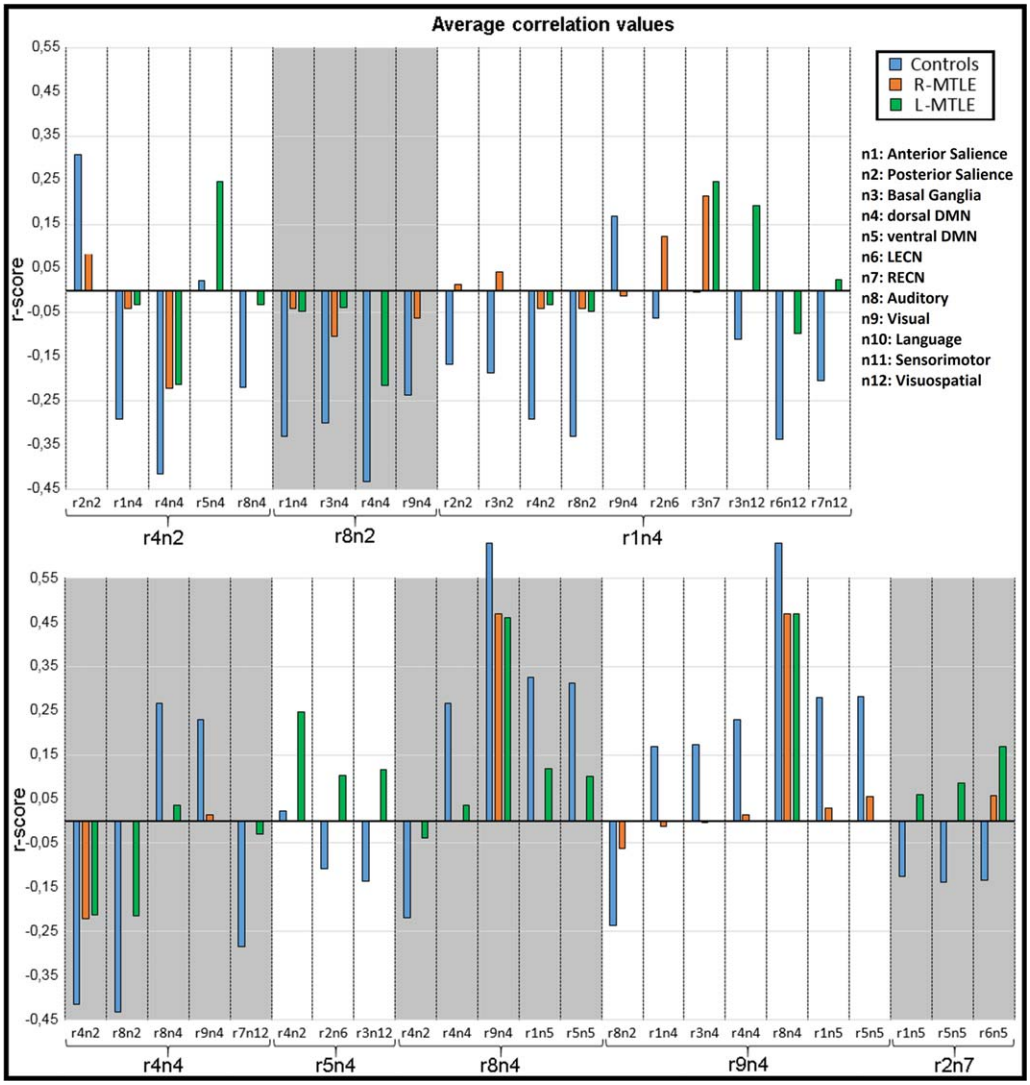

Figure 4.

Average correlation values of all (in hubs) altered connections organized by the nine alteration hubs and theirs existent altered connections. R-MTLE: right mesial temporal lobe epilepsy; L-MTLE: left mesial temporal lobe epilepsy.

RDAC (seven connections or 33% of the total number of alterations for each) whereas a relative low CCAC (0.1 for both). Conversely, posterior salience ROIs (r2n2, r4n2 and r8n2) and the ipsilateral superior frontal gyrus (DMN, r3n4) presented highest CCAC whereas lower RDAC. The LI of the R-MTLE group was 0.190 indicating that the majority of the R-MTLE alterations is ipsilateral, but also there are altered connections on the contralateral side.

L-MTLE Connectivity

In total, 29 ROIs linked by 28 connections showed alterations on L-MTLE group when compared to controls. We found five hubs with relative decreased connectivity including left hippocampus (r9n4), affecting connections with ventral and dorsal DMN ROIs (r4n4, r9n4, r1n5, and r5n5) and ipsilateral posterior salience (r4n2). The frontal portion of DMN (r1n4) and the bilateral inferior parietal gyrus of the posterior salience network (r8n2 and r4n2) were also hubs with deceased connections.

By a network perspective, we observed decreased intranetwork connectivity only between dorsal DMN (n4) ROIs. We found reductions on internetwork connectivity between posterior salience (n2) and dorsal DMN (n4) ROIs and also between dorsal DMN (n4) with ventral DMN (n5) and visuospatial/dorsal attention network (n12) (Table IV and Fig. 3B in blue lines).

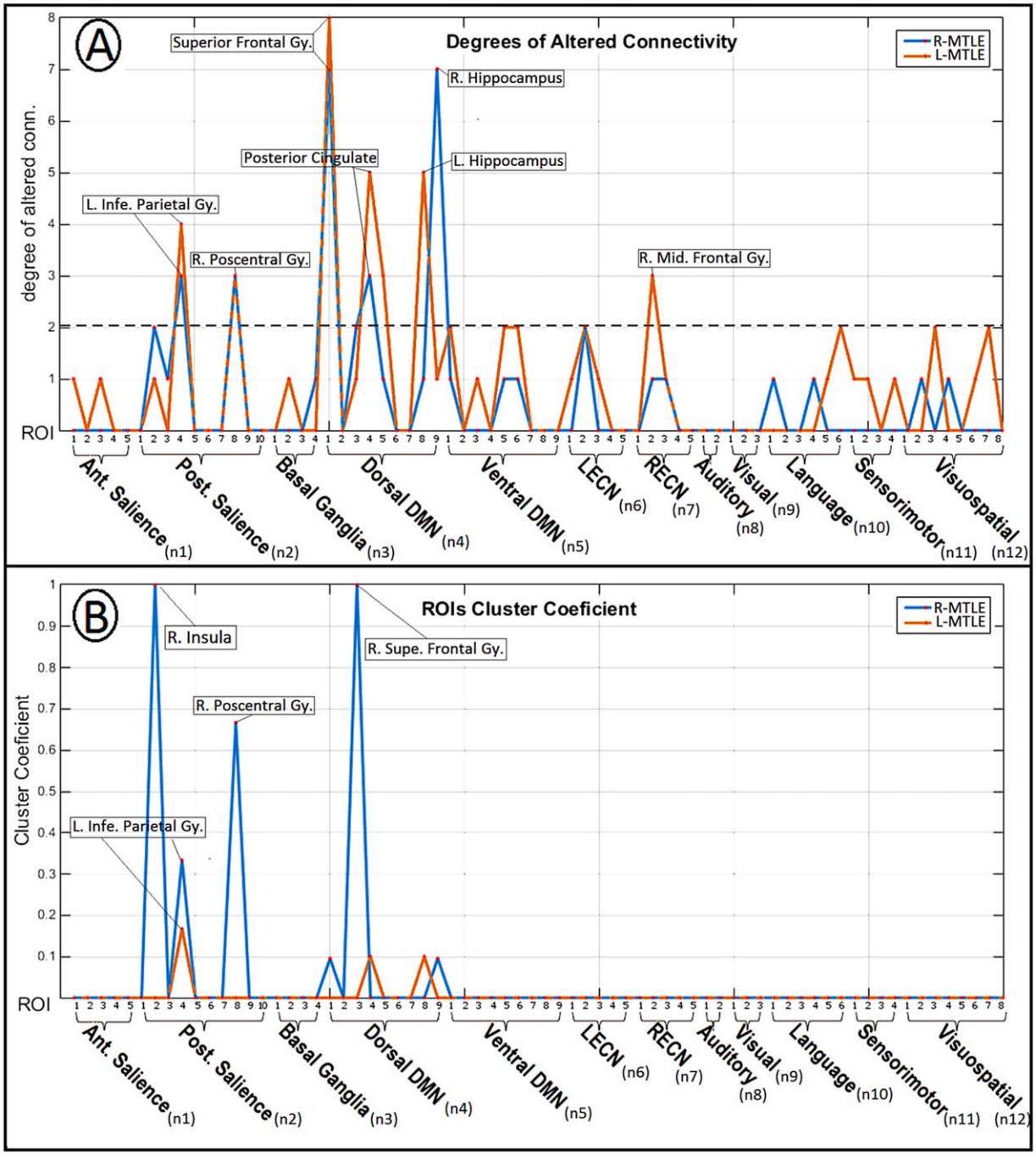

Figure 5.

ROIs graph theoretical results. In "**A**," the degree of altered connectivity (RDAC) and in "**B**" the cluster coefficient values (CCAC). The horizontal dashed lines in A, represents the ADAC that we used to define a ROIs with higher values as a hub of alterations. The dashed blue and yellow lines were used to indicate overlapping between groups lines. Conn.: connectivity; R-MTLE: right mesial temporal lobe epilepsy; L-MTLE: left mesial temporal lobe epilepsy; R: right; L: left; Gy: gyrus; Infe: inferior; Mid.: middle; Supe.: superior; Ant.: anterior; Post. Posterior; DMN: default mode network; LECN: left executive control network; RECN: right executive control network.

Three hubs presented relative increased connectivity: two dorsal DMN regions, the posterior cingulate (r4n4), bilateral thalamus (r5n4), and the ipsilateral inferior parietal gyrus (r4n2) of posterior salience. We observed increased internetwork connectivity between dorsal DMN (n4) and posterior salience (n2) ROIs and between sensorimotor (n11) and dorsal DMN (n4) ROIs (Table V and Fig. 3B in red lines).

We also observed opposite connectivity (relative to controls) on the L-MTLE group, which included a hub of the right ECN (r2n7) and only its connections with ventral DMN ROIs (r1n5, r5n5 and r6n5). Additionally, we found opposite connectivity on the frontal portion of dorsal DMN (r1n4) with bilateral inferior parietal gyri of the visuospatial/dorsal attention network (r3n12 and r7n12), ventral DMN (r6n5), right ECN (r3n7), and left posterior salience (r2n2). The thalamus (r5n4) was also considered a hub with opposite connections, which included visuospatial (r3n12) and left ECN (r2n6) networks ROIs (Table VI and Fig. 3B in dashed lines). By a network perspective, we found internetwork opposite connectivity alterations that involved the dorsal DMN (n4) with the posterior salience (n2), ventral DMN (n5), left and right ECN (n6 e n7), and visuospatial (n12). Additionally, we observed alterations between the right ECN (n7) and the ventral DMN (n5). The average connectivity values of all described altered connections are shown on Figure 4.

Graph theory properties

The L-MTLE group presented relevant RDAC on the frontal portion of the DMN (r1n4), in the posterior cingulate cortex (r4n4) and in the ipsilateral hippocampus (r8n4) (Fig. 5A). The CCAC in this group, revealed low clustering values with the highest score on the ipsilateral inferior parietal lobule (r4n2) (Fig. 5B).The LI for the L-MTLE group was 0.035 indicating that the majority of the L-MTLE alterations is ipsilateral but with a very similar quantity on the contralateral side.

DISCUSSION

Using resting-state fMRI, we investigated the patterns of connectivity alterations in patients with left and right MTLE. We performed several approaches of validated methodologies to extract clear information about each MTLE type separately. We demonstrated that patients with right and left MTLE have widespread abnormal interactions of large-scale networks. Despite the vast alteration in both patients groups, all evaluated parameters indicate that L-MTLE is a more intricate bilateral functional syndrome than R-MTLE. Moreover, ipsilateral hippocampi of both groups behave as central hubs of decreased functional connectivity.

The large-scale networks interaction abnormalities of L-MTLE and R-MTLE can be summarized as follows: (i) both R-MTLE and L-MTLE patients presented decreased connectivity and inversion of the correlation signal between the dorsal DMN and the posterior salience network (compared to controls); (ii) both R-MTLE and L-MTLE patients presented inversion of the correlation signal between the dorsal DMN and the ECN; (iii) L-MTLE patients presented decreased connectivity and inversion of the correlation signal between the dorsal DMN and the visuoespatial/dorsal attention network; (iv) in patients with L-MTLE, a relative increased connectivity was observed between the bilateral thalami and the posterior salience network.

Differences on connectivity alterations between left and right MTLE have been previously described in the literature [Haneef et al., 2015; Pereira et al., 2010; Waites et al., 2006]. Through diversified methodologies, these studies explored distinct aspects of brain functional connectivity using anatomical or functional relevant ROIs, independent component analysis and graph theoretical information. Our study unified some of these methodologies, applying consecutive techniques with an unbiased pipeline, providing robust results through an innovative point of view.

Abnormal Connectivity in Right and Left MTLE

For both groups, we found abnormal DMN connections, with the superior and middle frontal gyri as important hubs of alterations. The ipsilateral hippocampi was also highlighted as a central area of abnormalities, as expected due to its dominant importance in MTLE underlying physiopathology.

Differences of abnormal connectivity between right and left MTLE

With the exception of the ipsilateral hippocampi (that are altered according to the group lateralization), all hubs with relative decreased connectivity observed on R-MTLE patients were also observed on L-MTLE. In addition, patients with L-MTLE presented as hubs of relative decreased connectivity the dorsal DMN (r4n4) and the right ECN (r2n7). The idea that the L-MTLE patients are more susceptible to bilateral and diffuse structural alterations was already described in the literature [Ahmadi et al., 2009, Coan et al., 2009] and our study suggests that these patterns occurs also with the functional organization, involving contralateral networks. These findings are sustained by the laterality index that showed more ipsilateral-restricted alterations on R-MTLE, while the L-MTLE presented a more bilateral pattern of alterations.

In addition to the diffuse and bilaterally affected connectivity, the cluster-coefficient on the L-MTLE proved to be lower than in R-MTLE. This finding suggests that despite L-MTLE patients having a higher ADAC and widespread alterations, these abnormal connections presented low interactions between themselves. These facts could be related to the cognitive abnormalities presented in patients

with MTLE and in an ineffective attempt to restore these functionalities. On the R-MTLE patients, the ADAC was lower than in L-MTLE, with more restricted pattern of alterations including eight networks. Conversely, these alterations demonstrated to be integrated between themselves, with higher cluster coefficients and more ipsilaterally distributed as mentioned above. The clinical relevance of these findings, at this point, can only be speculative. Nevertheless, it is widely known that patients with L-MTLE have worse cognitive performance than R-MTLE [Alessio et al., 2006; Hermann et al., 1997]. As also suggested by intracranial EEG studies, the abnormal connectivity in the hemisphere contralateral to the epileptogenic zone in L-MTLE could be an attempt to compensate the functional deficit, as the performance of working memory scores have been correlated to this increased contralateral connectivity [Bettus et al., 2009]. However, in our study while regions of increased connectivity were only observed in L-MTLE, the graph theory parameters showed low interactions between these nodes, which could indicate an ineffective connectivity. Therefore, we believe that, at this point, the hypothesis of the occurrence of areas of increased connectivity in L-MTLE as a compensatory mechanism requires further investigation.

The connectivity within DMN ROIs is extensively reduced, with the ipsilateral hippocampus as a main hub of alterations for both groups, differing only on the opposite connectivity with the frontal portion of DMN (r1n4 and r3n) on the R-MTLE. The connectivity reduction between these areas could be secondary to the structural abnormalities as well as both ictal and interictal activities, closely related to the hippocampal damage [Zhang et al. 2010].

We also observed several internetworks alterations in R-MTLE and L-MTLE. Differently from previous studies, we assessed the internetworks abnormalities looking at positive and negative correlations and also at the inversion of the correlation directions between patients and controls, providing a full characterization of the abnormal interaction of the different brain regions in MTLE. In our study, both R-MTLE and L-MTLE patients presented altered correlations involving the DMN, the salience network and ECN, showing an inversion of the correlation signal between them in comparison to the control group. The Figure 3B reveals, for example, that an ECN hub (r2n7) of L-MTLE patients worked positively correlated with the DMN during rest, in opposite to the controls. Accordingly, both inferior frontal gyrus (both sides, r3n12 and r7n12) and the frontal portion of the DMN (r1n4) proved to be positively correlated, also in contrast to controls. The relationship between DMN, salience and ECNs is under investigation, but recent studies defined that DMN and salience work oppositely, meaning that the increase of the first is followed by a decrease in the second, and vice-versa [Balthazar, et al., 2014]. Some authors suggest that this mechanism involves a mediation of activity executed by the salience network guiding the focus on internal (DMN) or external (ECN) process and stimulus [Liang et al., 2016].

Other internetwork alterations were observed exclusively in L-MTLE, more specifically between DMN and visuospatial/dorsal attention network, which also presented an inversion of correlation signal. Previous studies demonstrated that the relation between DMN and visuospatial/dorsal attention network is supposedly anti-correlated [Tomasi et al., 2009], once the DMN should deactivate when the visuospatial is required to focus in a task. Since our study performed the functional acquisitions during rest, we can determine that visuospatial/dorsal attention network regions (r3n12 and r7n12) are misleadingly recruited by DMN, corroborating the evidence of a more disorganized functional behavior on L-MTLE. Additionally, only in patients with L-MTLE an increased connectivity was observed between the bilateral thalami and the posterior salience network, more specifically, the left inferior parietal region.

Although extensively described, the causes of diffuse abnormal functional and structural abnormalities in MTLE are unknown. One possible factor involved on RSN disruption in MTLE patients may be the underlying interictal activity. Although we do not have concomitant EEG recordings to this data, previous studies described the functional alterations caused by interictal spikes [Coan et al., 2014a]. However, there is no evidence that the characteristics of interictal epileptiform discharges, including rate, localization or extent, differ between right or left MTLE and, accordingly, these differences were also not observed between our groups of patients. Therefore, while the epileptiform discharges might affect the overall connectivity in MTLE patients, it might not contribute specifically to the differences between right and left MTLE. Similarly, while the chronic use of anti-epileptic drugs (as described for patients in use of topiramate [Yasuda et al., 2013]), as well as the natural disease evolution may also be relevant factors influencing connectivity abnormalities in MTLE, they may not necessarily impact the differences between right and left MTLE described in our study. These characteristics were balanced between the patients groups. Further prospective studies will be necessary to address the influence of these factors on connectivity alterations in MTLE.

Methodological Considerations

ROI-based studies applied to diseases with structural alteration such as hippocampal atrophy, should have additional attention during the time-series extractions. Misleading co-registration between the ROI mask and the cortex could include extra cortical tissues or regions with extensively altered cellular constitution that are not functionally representative. Although we did not include an atrophy mask as covariate in our model, the methodology applied for extraction of time series avoided confounding voxels through the tissue segmented mask and the required homogeneity among time-series from ROIs voxels.

The Figure 4 shows the average correlation values for each altered connection for each group. It is possible to identify means close to values related to noise (or non-significant average correlations: $P > 0.05$ or $r < 0.145$; with 180 degrees of freedom—number of dynamics for each run). Our aim was to include all possible not connected regions in the analysis, since we considered the possibility of the occurrence of convertion of absent connections into significant ones and vice-versa in MTLE. For instance, the connection between regions r1n4 and r3n7 is almost absent in controls subjects but it is consistently present in the R-MTLE and L-MTLE groups.

In this study, we applied established approaches as cross-correlation between series and graph theoretical parameters, but we also quantified these graph properties with the difference between MTLE groups and controls as a third level step. This method characterizes the patterns of alterations directly, avoiding arbitrary successive thresholds commonly applied on graph-theoretical studies.

The networks parcellation and nomination can vary among authors. Since we decided to use the Shirer's parcellation in our study, we strive to respect that organization with few exceptions (described on the "Methods"). These divergences are usually secondary to chosen parameters during the process to create the functional templates such as, for example, the defined number of components to be determined during an Independent Component Analysis. In our study, the dorsal attention network is represented by the Visuospatial (n12). Differently, a network exclusively composed by ROIs of the Ventral Attention network (VAN) is missing. We concluded that the regions composing the VAN are represented by ROIs included on the perceptual networks (e.g., sensorimotor, auditory). Therefore, despite not including the VAN, the relevant anatomical regions associated to it are considered in our ROI-wise analysis. We understand that the results presented on Tables (II–VI), can assist these interpretations, since they "translate" the functional ROI name to specific anatomical region.

The UF^{2}C toolbox demonstrated to be an efficient and straightforward tool to investigate functional connectivity. The minimalist user interface and the standard settings enable reliable assessment of functional information through a consistent and validated preprocessing pipeline.

CONCLUSION

Patients with right and left MTLE have widespread abnormal interactions of large-scale networks. Despite the vast alteration in both patients groups, all evaluated parameters indicate that L-MTLE has a more intense bihemispheric dysfunction compared to right-MTLE.

REFERENCES

Ahmadi ME, Hagler DJ Jr, McDonald CR, Tecoma ES, Iraguid VJ, Dale AM, Halgren E (2009): Side matters: Diffusion tensor imaging tractography in left and right temporal lobe epilepsy. AJNR 30:1740–1747.

Alessio A, Bonilha L, Rorden C, Kobayashi E, Min LL, Damasceno BP, Cendes F (2006): Memory and language impairments and their relationships to hippocampal and perirhinal cortex damage in patients with medial temporal lobe epilepsy. Epilepsy Behav 8:593–600.

Balthazar MLF, Pereira FRS, Lopes TM, da Silva EL, Coan AC, Campos BM, Duncan NW, Stella F, Northoff G, Damasceno BP, Cendes F (2014): Neuropsychiatric symptoms in Alzheimer's disease are related to functional connectivity alterations in the salience network. Hum Brain Mapp 35:1237–1246.

Benjamini Y, Hochberg Y (1995): Controlling the false discovery rate: A practical and powerful approach to multiple testing. J R Stat Soc Ser B (Methodological) 57:289–300.

Berg AT, Berkovic SF, Brodie MJ, Buchhalter J, Cross JH, Van Emde Boas W, Engel J, French J, Glauser TA, Mathern GW, Moshé SL, Nordli D, Plouin P, Scheffer IE (2010): Revised terminology and concepts for organization of seizures and epilepsies: Report of the ILAE Commission on Classification and Terminology, 2005–2009. Epilepsia 51:676–685.

Bernhardt BC, Chen Z, He Y, Evans AC, Bernasconi N (2011): Graph-theoretical analysis reveals disrupted small-world organization of cortical thickness correlation networks in temporal lobe epilepsy. Cereb Cortex 21:2147–2157.

Besson P, Dinkelacker V, Valabregue R, Thivard L, Leclerc X, Baulac M, Sammler D, Colliot O, Lehéricy S, Samson S, Dupont S (2014): Structural connectivity differences in left and right temporal lobe epilepsy. Neuroimage 100:135–144.

Bettus G, Guedj E, Joyeux F, Confort-Gouny S, Soulier E, Laguitton V, Cozzone PJ, Chauvel P, Ranjeva JP, Bartolomei F, Guye M (2009): Decreased basal fMRI functional connectivity in epileptogenic networks and contralateral compensatory mechanisms. Hum Brain Mapp 30:1580–1591.

Bonilha L, Helpern JA, Sainju R, Nesland T, Edwards JC, Glazier SS, Tabesh A (2013): Presurgical connectome and postsurgical seizure control in temporal lobe epilepsy. Neurology 81:1704–1710.

Bullmore E, Sporns O (2009): Complex brain networks: Graph theoretical analysis of structural and functional systems. Nat Rev Neurosci 10:186–198.

Campos BM, Coan AC, Beltramini GC, Liu M, Yassuda CL, Ghizoni E, Beaulieu C, Gross DW, Cendes F (2015): White matter abnormalities associate with type and localization of focal epileptogenic lesions. Epilepsia 56:125–132.

Cataldi M, Avoli M, de Villers-Sidani E (2013): Resting state networks in temporal lobe epilepsy. Epilepsia 54:2048–2059.

Cendes F, Andermann F, Gloor P, Lopes-Cendes I, Andermann E, Melanson D, Jones-Gotman M, Robitaille Y, Evans A, Peters T (1993): Atrophy of mesial structures in patients with temporal lobe epilepsy: Cause or consequence of repeated seizures? Ann Neurol 34:795–801.

Chiang S, Haneef Z (2014): Graph theory findings in the pathophysiology of temporal lobe epilepsy. Clin Neurophysiol 125: 1295–1305.

Coan AC, Appenzeller S, Bonilha L, Li LM, Cendes F (2009): Seizure frequency and lateralization affect progression of atrophy in temporal lobe epilepsy. Neurology 73:834–842.

Coan AC, Campos BM, Beltramini GC, Yasuda CL, Covolan RJM, Cendes F (2014a): Distinct functional and structural MRI abnormalities in mesial temporal lobe epilepsy with and without hippocampal sclerosis. Epilepsia 55:1187–1196.

Coan AC, Kubota B, Bergo FPG, Campos BM, Cendes F (2014b): 3T MRI quantification of hippocampal volume and signal in mesial temporal lobe epilepsy improves detection of hippocampal sclerosis. AJNR 35:77–83.

Coito A, Plomp G, Genetti M, Abela E, Wiest R, Seeck M, Michel CM, Vulliemoz S (2015): Dynamic directed interictal connectivity in left and right temporal lobe epilepsy. Epilepsia 56:207–217.

Eguíluz VM, Chialvo DR, Cecchi GA, Baliki M, Apkarian AV (2005): Scale-free brain functional networks. Phys Rev Lett 94: 018102.

Haneef Z, Lenartowicz A, Yeh HJ, Levin HS, Engel J Jr, Stern JM (2014): Functional connectivity of hippocampal networks in temporal lobe epilepsy. Epilepsia 55:137–145.

Haneef Z, Chiang S, Yeh HJ, Engel J Jr, Stern JM (2015): Functional connectivity homogeneity correlates with duration of temporal lobe epilepsy. Epilepsy Behav 46:227–233.

Hermann BP, Seidenberg M, Schoenfeld J, Davies K (1997): Neuropsychological characteristics of the syndrome of mesial temporal lobe epilepsy. Arch Neurol 54:369–376.

Holmes MJ, Yang X, Landman BA, Ding Z, Kang H, Abou-Khalil B, Sonmezturk HH, Gore JC, Morgan VL (2013): Functional networks in temporal-lobe epilepsy: A voxel-wise study of resting-state functional connectivity and gray-matter concentration. Brain Connect 3:22–30.

Keller SS, Mackay CE, Barrick TR, Wieshmann UC, Howard MA, Roberts N (2002): Voxel-based morphometric comparison of hippocampal and extrahippocampal abnormalities in patients with left and right hippocampal atrophy. Neuroimage 16:23–31.

Laufs H, Hamandi K, Salek-Haddadi A, Kleinschmidt AK, Duncan JS, Lemieux L (2007): Temporal lobe interictal epileptic discharges affect cerebral activity in "default mode" brain regions. Hum Brain Mapp 28:1023–1032.

Liang X, Yong Z, Yihong H, Yang Y (2016): Topologically reorganized connectivity architecture of default-mode, executive-control, and salience networks across working memory task loads. Cereb Cortex 26:1501–1511.

Liao W, Zhang Z, Pan Z, Mantini D, Ding J, Duan X, Luo C, Lu G, Chen H (2010): Altered functional connectivity and small-world in mesial temporal lobe epilepsy. PLoS One 5:e8525.

Liao W, Zhang Z, Pan Z, Mantini D, Ding J, Duan X, Luo C, Wang Z, Tan Q, Lu G, Chen H (2011): Default mode network abnormalities in mesial temporal lobe epilepsy: A study combining fMRI and DTI. Hum Brain Mapp 32:883–895.

Liu M, Concha L, Lebel C, Beaulieu C, Gross DW (2012): Mesial temporal sclerosis is linked with more widespread white matter changes in temporal lobe epilepsy. Neuroimage Clin 1:99–105.

Morgan VL, Sonmezturk HH, Gore JC, Abou -Khalil B (2012): Lateralization of temporal lobe epilepsy using resting functional magnetic resonance imaging connectivity of hippocampal networks. Epilepsia 53:1628–1635.

Pereira FR, Alessio A, Sercheli MS, Pedro T, Bilevicius E, Rondina JM, Ozelo HF, Castellano G, Covolan RJ, Damasceno BP, Cendes F (2010): Asymmetrical hippocampal connectivity in mesial temporal lobe epilepsy: Evidence from resting state fMRI. BMC Neurosci 11:66.

Pittau F, Grova C, Moeller F, Dubeau F, Gotman J (2012): Patterns of altered functional connectivity in mesial temporal lobe epilepsy. Epilepsia 53:1013–1023.

Riederer F, Lanzenberger R, Kaya M, Prayer D, Serles W, Baumgartner C (2008): Network atrophy in temporal lobe epilepsy A voxel-based morphometry study. Neurology 71:419–425.

Rubinov M, Sporns O (2010): Complex network measures of brain connectivity: Uses and interpretations. NeuroImage 52:1059–1069.

Seeley WW, Crawford RK, Zhou J, Miller BL, Greicius MD (2009): Neurodegenerative diseases target large-scale human brain networks. Neuron 62:42–52.

Shirer WR, Ryali S, Rykhlevskaia E, Menon V, Greicius MD (2012): Decoding subject-driven cognitive states with whole-brain connectivity patterns. Cereb Cortex. 22(1):158–165.

Spencer SS (2002): Neural networks in human epilepsy: Evidence of and implications for treatment. Epilepsia 43:219–227.

Tomasi D, Volkow ND, Wang R, Telang F, Wang G-J, Chang L, Ernst T, Fowler JS. (2009): Dopamine transporters in striatum correlate with deactivation in the default mode network during visuospatial attention. PLoS One 4:e6102.

Vannest J, Szaflarski JP, Privitera MD, Schefft BK, Holland SK (2008): Medial temporal fMRI activation reflects memory lateralization and memory performance in patients with epilepsy. Epilepsy Behav 12:410–418.

Vlooswijk MC, Vaessen MJ, Jansen JF, de Krom MC, Majoie HJ, Hofman PA, Aldenkamp AP, Backes WH (2011): Loss of network efficiency associated with cognitive decline in chronic epilepsy. Neurology 77:938–944.

Waites AB, Briellmann RS, Saling MM, Abbott DF, Jackson GD (2006): Functional connectivity networks are disrupted in left temporal lobe epilepsy. Ann Neurol 59:335–343.

Wang J, Wang L, Zang Y, Yang H, Tang H, Gong Q, Chen Z, Zhu C, He Y (2009): Parcellation-dependent small-world brain functional networks: A resting-state fMRI study. Hum Brain Mapp 30:1511–1523.

Yasuda CL, Centeno M, Vollmar C, Stretton J, Symms M, Cendes F, Mehta MA, Thompson P, Duncan JS, Koepp MJ (2013): The effect of topiramate on cognitive fMRI. Epilepsy Res 105:250–255.

Zhang Z, Lu G, Zhong Y, Tan Q, Liao W, Chen Z, Shi J, Liu Y (2009a): Impaired perceptual networks in temporal lobe epilepsy revealed by resting fMRI. J Neurol 256:1705–1713.

Zhang Z, Lu G, Zhong Y, Tan Q, Yang Z, Liao W, Chen Z, Shi J, Liu Y (2009b): Impaired attention network in temporal lobe epilepsy: A resting FMRI study. Neurosci Lett 458:97–101.

Zhang Z, Lu G, Zhong Y, Tan Q, Liao W, Wang Z, Wang Z, Li K, Chen H, Liu Y (2010): Altered spontaneous neuronal activity of the default-mode network in mesial temporal lobe epilepsy. Brain Res 1323:152–160.